Optical properties of quaternary GaInAsSb/AlGaAsSb strained quantum wells

1996 J. Phys.: Condens. Matter 8 4751

(http://iopscience.iop.org/0953-8984/8/26/007)

J. Phys.: Condens. Matter **8** (1996) 4751–4766. Printed in the UK

Optical properties of quaternary GaInAsSb/AlGaAsSb strained quantum wells

W Z Shen†, S C Shen†, W G Tang†, Y Chang†, Y Zhao‡ and A Z Li‡

† CCAST (World Laboratory), PO Box 8730, Beijing 100080, and National Laboratory for Infrared Physics, Shanghai Institute of Technical Physics, Shanghai 200083, People's Republic of China§

‡ Department of Functional Materials for Informatics, Shanghai Institute of Metallurgy, Shanghai 200050, People's Republic of China

Received 16 January 1996, in final form 12 March 1996

Abstract. The electronic states in quaternary GaInAsSb/AlGaAsSb strained quantum well (QW) structures grown by molecular beam epitaxy have been investigated both theoretically and experimentally. For $Ga_{0.75}In_{0.25}As_{0.04}Sb_{0.96}/Al_{0.22}Ga_{0.78}As_{0.02}Sb_{0.98}$ strained multiple quantum wells (MQWs), strong luminescence, and well-resolved excitonic absorption peaks are observed even at room temperature, which is indicative of the good quality of our quaternary sample. By fitting the experimental results to the theoretical calculations, we find that the light holes are in $Ga_{0.75}In_{0.25}As_{0.04}Sb_{0.96}$ well regions (type I MQWs) and the conduction band offset ratio $Q_c = 0.66 \pm 0.01$. The critical temperature for the excitonic-polariton–mechanical-exciton transition in this quaternary MQW structure was found to be ∼40 K. The measured intersubband absorption of about 10.7 μm is in good agreement with the theoretical calculation. The transition from type I MQWs to type II MQWs for light holes is also predicted theoretically. In the photoluminescence spectra the sharp exciton resonances have been attributed to localized excitons for temperature ⩽80–100 K and to free excitons at higher temperatures up to room temperature. We conclude that the dominant luminescence quenching mechanism in this quaternary system is mainly that of the trapped excitons thermalizing from the localized regions below 100 K, and the thermal carrier activation from the first electron and heavy-hole subbands to the second electron and heavy-hole subbands at higher temperatures. The strength of the exciton–phonon coupling is determined from the linewidth analysis. The inhomogeneous linewidth and homogeneous broadening in both MQW and single-quantum-well (SQW) structures have been discussed. We conclude that the experimental result of stronger exciton–phonon coupling in the quaternary SQW structure will lead to partial ionization of excitons at higher temperatures (above 125 K), in good agreement with the line-shape analysis of the luminescence spectra which clearly shows the presence of band-to-band recombination.

1. Introduction

Advancement in the field of semiconductor growth has enabled us to prepare various artificial structures both for fundamental studies and for device applications. Recently, much attention has been devoted to the study of optical properties of two-dimensional systems such as QW structures as a consequence of their great importance for the development of new electro-optical devices [1]. One of the most interesting properties in QW structures is the appearance of sharp, well-resolved exciton peaks in the photoluminescence (PL) and absorption spectra at room temperature (at which most devices should be used), while the corresponding

§ Mailing address.

0953-8984/96/264751+16$19.50

bulk material shows exciton peaks just at very low temperatures. This is due to the low-dimensional characteristics, i.e., space restriction of wave functions and increase of exciton binding energy in two-dimensional systems. Therefore, exciton recombination plays a much more important role in QW structures than that in bulk materials, which highlights the need to fully understand the carrier dynamics and exciton recombination processes in QW structures. PL is established as an important characterization tool for these recombination processes, as well as for assessing the QW quality. The main PL quenching mechanism in QW structures has been attributed by some authors [2–4] to thermal carrier activation from the wells into barriers, followed by nonradiative recombination in the barriers, while other authors [5–7] emphasize the importance of the carrier or exciton trapping at the QW interface defects.

GaInAsSb/AlGaAsSb quaternary QW systems have recently received much attention, due to their potential application as semiconductor diode lasers with emission wavelength in the range 2–4 μm, which is currently of great interest since here they match with recent development of low-loss fluoride glass fibres in this spectral region [8–13]. Room-temperature operation of lattice-matched GaInAsSb/AlGaAsSb lasers grown by both liquid-phase epitaxy (LPE) [10, 11] and molecular beam epitaxy (MBE) [12, 13] has been demonstrated. However, detailed investigation of the PL characteristics for these quaternary QW systems has not been reported. The recombination of photoexcited carriers in GaInAsSb/AlGaAsSb QW is a process of vital importance for the optoelectronic devices based on these quaternary QW structures. On the other hand, the employment of strained quantum wells in devices extends the choice of compatible materials and greatly increases the extent to which one can control their optical and electronic properties. Recent investigations show that the strained MQW laser diodes may be superior to those with conventional unstrained MQW structures in operational characteristics.

Further motivation for studying GaInAsSb/AlGaAsSb structures here is provided by the fact that the fundamental properties, including some important parameters of this quaternary system, are less fully investigated. Adachi [14, 15] has presented a number of important material parameters for the quaternary systems, e.g., the band gaps, effective masses, and refractive index. The strain, band offsets, and subband behaviour of the GaInAsSb/AlGaAsSb quaternary system are still lacking. Photoluminescence excitation spectra yield direct insight into the semiconductor optical properties at different temperatures without requiring one to consider the luminescence efficiency at high temperatures. In the absence of a tunable laser source with a wavelength suitable for the measurements—which would be necessary for absorption measurements—absorption measurements are very suitable for studying the above parameters. Also, absorption measurements can give additional valuable information, e.g., on the excitonic linewidth, exciton–phonon coupling, and intersubband transitions. Excitonic linewidths, both homogeneous and inhomogeneous, as well as exciton–phonon coupling, are of critical importance to the performance of quantum-well-based modulation devices [16], and the results on infrared intersubband transitions within the conduction band of the quantum well can be applied to quantum well infrared photodetectors (QWIPs) [17, 18]. Better understanding of these important physical parameters would be helpful in optoelectronic device development.

This paper reports on the detailed PL and absorption spectra for both MQW and SQW GaInAsSb/AlGaAsSb structures. Following the introduction, the experiments are briefly described in section 2. Section 3 gives the detailed calculation procedure for the strained quaternary structures. The observation of spectra and a discussion are presented in section 4.

2. Experiment details

The quaternary GaInAsSb/AlGaAsSb QW structures used in the optical measurements were grown by the MBE technique on (100)-oriented n^+ GaSb substrate. A 1.0 μm lattice-matched n^+ (1.0×10^{18} cm^{-3}) $Al_{0.22}Ga_{0.78}As_{0.02}Sb_{0.98}$ buffer layer was grown first on the substrate. The MQW structure was composed of twenty periods amounting to 10 nm of undoped $Ga_{0.75}In_{0.25}As_{0.04}Sb_{0.96}$ well and 30 nm of undoped $Al_{0.22}Ga_{0.78}As_{0.02}Sb_{0.98}$ barrier layer. The SQW sample contained a single AlGaAsSb/GaInAsSb/AlGaAsSb QW structure and had the same well and barrier width as the MQW sample, i.e., a $Ga_{0.67}In_{0.33}As_{0.01}Sb_{0.99}$ well–layer structure 10 nm thick was placed between two $Al_{0.25}Ga_{0.75}As_{0.02}Sb_{0.98}$ cladding layers that were 30 nm thick. All of the layers were undoped. The growth temperature for the epitaxy layers was 520 °C. The compositions were determined by an electron microprobe analysis, while the layer thicknesses were estimated from the growth rate. They were confirmed further by double-crystal x-ray diffraction measurements.

PL and absorption measurements were performed on a Nicolet 800 Fourier transform infrared spectrometer over the temperature range of 4.0 K to room temperature (290.0 K). The PL measurements were carried out using an Ar-ion (514.5nm) laser for excitation and a liquid-nitrogen-cooled InSb detector, while the absorption spectra were detected with a liquid-nitrogen-cooled InSb photodiode (or a HgCdTe photodiode for intersubband absorption) with a tungsten (or Globar for intersubband absorption) lamp focused onto the sample. The optical measurements were made at the resolution of 4 cm^{-1}.

3. Theory

The temperature-dependent band gaps of quaternary alloy $A_xB_{1-x}C_yD_{1-y}$ structures can be calculated from the following equation [14]:

$$E_g(x, y, T) = \frac{E_{g1} + E_{g2}}{x(1-x) + y(1-y)}$$

with

$$\begin{aligned} E_{g1} &= x(1-x)[yE_{gABC}(x, T) + (1-y)E_{gABD}(x, T)] \\ E_{g2} &= y(1-y)[xE_{gACD}(y, T) + (1-x)E_{gBCD}(y, T)] \end{aligned} \tag{1}$$

where the ternary alloy band gaps (namely: $E_{gABC}(x, T)$, $E_{gABD}(x, T)$, $E_{gACD}(y, T)$ and $E_{gBCD}(y, T)$) can be expressed in the form of quadratic functions, for example

$$E_{gABC}(x, T) = xE_{gAC}(T) + (1-x)E_{gBC}(T) + Bx(x-1) \tag{2}$$

while the bowing parameters B and temperature-dependent binary energy gaps are given in the literature [14, 19]. In ternary alloys constituted from lattice-mismatched binaries, bowing effects should be taken into account.

The other quaternary material parameters $P(x, y)$, e.g., lattice constants, and effective masses, are approximated as being temperature independent and can be estimated from these binary parameters (P) by using the linear interpolation scheme:

$$P(x, y) = xyP_{AC} + x(1-y)P_{AD} + (1-x)yP_{BC} + (1-x)(1-y)P_{BD} \tag{3}$$

for the binary values, which are summarized in table 1.

The details of the strain-induced changes to the band structure of layer semiconductor structures have been investigated by Pollak *et al* (see [20, 21]) and will only be briefly reviewed here. In our quantum well case, the GaInAsSb wells suffer biaxial in-plane compressive strain, while the AlGaAsSb barriers can be regarded as unstrained. The strain

Table 1. Parameters used in calculating the quaternary QW transition energies. All of the values are taken from [14], [15], [21], [33], and [34], except as indicated by footnotes.

	a_0 (nm)	a (eV)	b (eV)	Δ (eV)	C_{11} (10^{11} dyn cm^{-2})	C_{12} (10^{11} dyn cm^{-2})	m_e^*/m_0	m_{hh}^*/m_0	m_{lh}^*/m_0	E_{ph} (meV)
GaAs	0.5653	−8.68	−1.7	0.341	11.88	5.38	0.067	0.45	0.074	36.1
InAs	0.6058	−5.91	−1.8	0.381	8.33	4.53	0.023	0.41	0.028	30.2
AlAs	0.5661	−7.96	−1.5	0.275	12.02	5.70	0.150	0.76	0.150	—
GaSb	0.6095	−8.30[a]	−1.8[a]	0.820[b]	9.00	3.98	0.046	0.39[c]	0.046	29.5
InSb	0.6480	−7.70[a]	−2.1[a]	0.810[b]	6.76	3.48	0.016	0.18[c]	0.016	24.7
AlSb	0.6136	−5.90[a]	−1.4[a]	0.650[b]	9.02	4.45	0.110[c]	0.39[c]	0.110	42.2

[a] From [35].
[b] From [36].
[c] From [37].

ϵ of the GaInAsSb layers is determined as the relative difference in lattice constants of the well and barrier layers, and is given by

$$\epsilon = (a_{AlGaAsSb} - a_{GaInAsSb})/a_{GaInAsSb}. \tag{4}$$

An accurate description of the valence band manifolds under strain is given by a 6×6 Hamiltonian. In QWs, the lattice mismatch is accommodated by elastic strain in the well layers; the barrier layers remain unstrained. For growth in the (001) direction, the increase of the band gap of the GaInAsSb wells due to the biaxial compression can be obtained by diagonalizing a reduced 3×3 Hamiltonian, which yields three eigenvalues at $k = 0$:

$$\Delta E_{hh} = E_H + E_S \tag{5}$$

$$\Delta E_{lh} = E_H + \frac{1}{2}(\Delta - E_S - \sqrt{\Delta^2 + 2\Delta E_S + 9E_S^2}) \tag{6}$$

$$\Delta E_{so} = E_H + \frac{1}{2}(\Delta - E_S + \sqrt{\Delta^2 + 2\Delta E_S + 9E_S^2}) \tag{7}$$

with

$$\begin{aligned} E_H &= 2a\frac{C_{11} - C_{12}}{C_{11}}\epsilon \\ E_S &= -b\frac{C_{11} + 2C_{12}}{C_{11}}\epsilon \end{aligned} \tag{8}$$

for the heavy-hole valence band, the light-hole valence band, and the spin–orbit split-off band, respectively. In the above equations, a is the hydrostatic deformation potential, b is the shear deformation potential, C_{11} and C_{12} are the elastic stiffness constants, and Δ is the spin–orbit splitting energy. The above energy band components of the quaternary alloys are obtained by linear interpolation (equation (3)) of the binary values.

In addition to the strain-induced renormalization of the energy bands, we should also take into account the electron and hole confinements. The confinement energies for SQW structures can be calculated by using a standard finite square-well model, while for MQW structures they are treated with standard procedures which are based on an application of the Kronig–Penney model:

$$\cos(kl) = \cos(k_w l_w)\cosh(k_b l_b) + \frac{1}{2}\left(c - \frac{1}{c}\right)\sin(k_w l_w)\sinh(k_b l_b) \tag{9}$$

where l_w and l_b are the well and barrier widths, $l = l_w + l_b$ is the quantum well period, and

$$c = \frac{k_b m_w}{k_w m_b}$$
$$\hbar k_w = \sqrt{2m_w E} \qquad \hbar k_b = \sqrt{2m_b(\Delta E_{c(v)} - E)} \tag{10}$$

where m_w and m_b are the effective masses in the well and barrier layers, and $\Delta E_{c(v)}$ is the potential barrier height corresponding to conduction (valence) band offset after taking into account the strain effects:

$$\Delta E_c + \Delta E_v = E_b - E_w$$
$$Q_c = \frac{\Delta E_c}{\Delta E_c + \Delta E_v} \tag{11}$$

where E_b and E_w are energy gaps of the barrier and well layers, and Q_c is defined as the conduction band offset ratio.

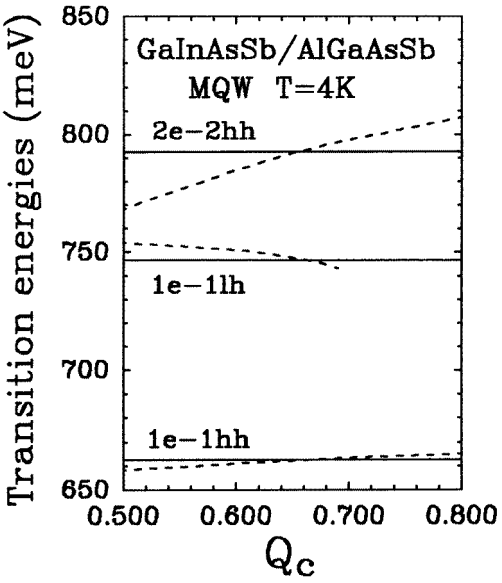

Figure 1. Calculated transition energies at 4.0 K (dashed curves) as functions of the conduction band offset ratio Q_c for a $Ga_{0.75}In_{0.25}As_{0.04}Sb_{0.96}/Al_{0.22}Ga_{0.78}As_{0.02}Sb_{0.98}$ strained MQW structure. The experimental results for excitonic absorption are shown by solid lines.

The energy of the free-exciton transitions between the nth electron subband and mth heavy-hole (ne–$m$hh) or light-hole (ne–$m$lh) subband of GaInAsSb wells can be expressed as

$$E^{theor}_{ne-mhh} = E_{g0} + \Delta E_{hh} + E_{ne} + E_{mhh} - E_{bhh}$$
$$E^{theor}_{ne-mlh} = E_{g0} + \Delta E_{lh} + E_{ne} + E_{mlh} - E_{blh} \tag{12}$$

where E_{g0} is the unstrained energy gap of GaInAsSb wells, and E_{ne}, E_{mhh}, and E_{mlh} are the nth electron, mth heavy-hole, and mth light-hole confinement energies, respectively. E_{bhh} and E_{blh} are the heavy-hole and light-hole excitonic binding energies.

Figure 1 displays the calculated transition energies for the excitons of the MQW sample at 4.0 K (dashed curves) as functions of the conduction band offset ratio Q_c, together

with the absorption results, shown by the solid lines. The excitonic binding energies were estimated all to be ∼10 meV for our 10 nm wells. In calculating the light-hole confinement energies, the potential barrier height has to be referenced to the light-hole band edge, i.e., it is decreased by $\Delta E_{lh} - \Delta E_{hh}$. Therefore, with increasing Q_c, the potential barrier height will become smaller than 0; that is, the light-hole valence band may become type II (confined in the AlGaAsSb barrier regions) due to the band splitting of heavy- and light-hole subbands induced by the strain, which was not shown in figure 1.

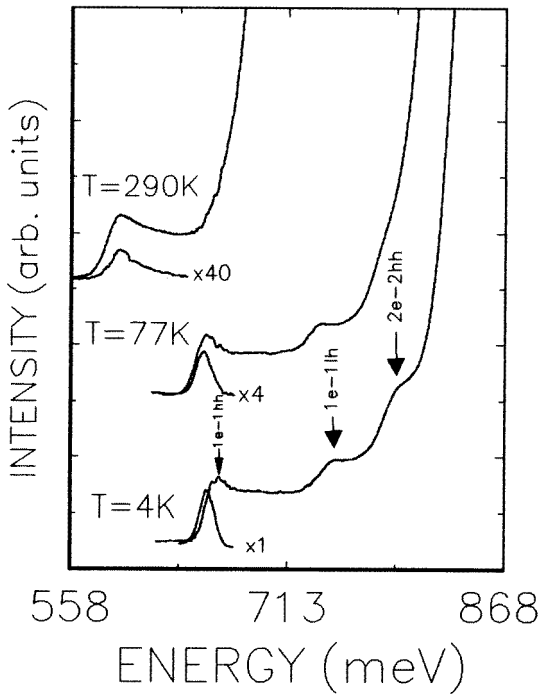

Figure 2. Temperature-dependent photoluminescence and absorption spectra for the quaternary $Ga_{0.75}In_{0.25}As_{0.04}Sb_{0.96}/Al_{0.22}Ga_{0.78}As_{0.02}Sb_{0.98}$ strained MQW structure. The laser power density was 100 mW cm^{-2} for the PL measurements. The magnification factors are marked only for PL spectra. Each spectrum set has been shifted up by a constant, for clarity.

4. Results and discussion

4.1. Band offsets

Figure 2 shows the PL and absorption spectra at different temperatures for the strained $Ga_{0.75}In_{0.25}As_{0.04}Sb_{0.96}/Al_{0.22}Ga_{0.78}As_{0.02}Sb_{0.98}$ MQW sample. In the PL spectra, a single PL peak is observed, corresponding to the recombination between the first electron subband and the first heavy-hole subband (1e–1hh), throughout the temperature region of the measurements (4.0–290.0 K), with a full width at half-maximum (FWHM) of ∼12.1 meV at 4.0 K and 22.1 meV at 290.0 K. This experimental result is consistent with the fact that only one strong luminescence peak can be observed in GaInAsSb layers with compositions closer to or inside the miscibility region grown by nonequilibrium techniques,

such as organometallic vapour-phase epitaxy (OMVPE) and MBE [22, 23]. Furthermore, we have observed nearly complete suppression of the luminescence from the AlGaAsSb barriers indicating very efficient charge transfer to the GaInAsSb quantum wells, with implications for optical devices. However, in absorption spectra, additional excitonic absorption structures (1e–1lh and 2e–2hh) appear at lower temperatures due to the increase of the overlap integral of the electron and hole wave functions. (The notation ne–mh(l)h indicates the transitions between the nth conduction and the mth valence heavy- (light-) hole subband.) The sharp rise in the highest-energy portion of the absorption spectra is due to absorption in the GaSb substrate, which was only polished but not removed. Strong luminescence and well-resolved excitonic absorption peaks are observed even at room temperature (290.0 K), which demonstrates the good quality of the quaternary structure. To the best of our knowledge, they have not been reported for GaInAsSb/AlGaAsSb MQW structures before.

A theoretical calculation was performed to identify the origin of the spectral features observed in the absorption spectra, marked in figure 2, and to extract the fundamental parameters of the structure from the measurements. Since the lowest transition (1e–1hh) energies are relatively insensitive to the value of the band offset used, the low-temperature absorption measurements give us more reliability in determining the band offsets (see below). We show the theoretical and experimental results in figure 1. The measured transition energies meet the calculated curves at positions which correspond to the real conduction band offset ratio Q_c of 0.66 ± 0.01. And the energy band configuration for light holes is confirmed to be type I (confined in the GaInAsSb well regions) for strained $Ga_{0.75}In_{0.25}As_{0.04}Sb_{0.96}/Al_{0.22}Ga_{0.78}As_{0.02}Sb_{0.98}$ MQW structures, which makes it possible to implement MQW-based lasers using this quaternary system. This is also the reason that one can observe strong excitonic resonance of the 1e–1lh transportation in absorption spectra (see figure 2). This conclusion is further supported by the better agreement with the experimental results when we choose the 1e–1lh transitions to be excitonic rather than band-to-band transitions in the calculations. And furthermore, the same conclusion was obtained for all of the temperature-dependent PL and absorption measurements.

4.2. Light-hole behaviour

On changing the compositions, e.g., increasing the indium composition, the strain within the quaternary structure will be increased, resulting in larger band splitting of heavy and light holes. Next we would like to study the transition from type I to type II quantum wells for light holes. On the basis of the band offsets determined above, our calculation shows that the transition may occur for x-values smaller than 0.70 in the quaternary $Ga_xIn_{1-x}As_{0.04}Sb_{0.96}/Al_{0.22}Ga_{0.78}As_{0.02}Sb_{0.98}$ MQW structures. Since the lattice mismatch can be fully accommodated by elastic deformation in the GaInAsSb well layers with the composition x-value between 0.65 and 0.75, this transition might be observed.

4.3. The origin of the PL emission

The Stokes shift between the PL and absorption peaks shows a temperature-dependent behaviour (see figure 2): there is relatively large Stokes shift at low temperatures, e.g., $\sim$8.0 meV at 4 K, and a small Stokes shift for temperatures above 100 K (within 2.0 meV), indicating luminescence of excitons localized at material defects [24, 25] such as disorder defects of quaternaries and misfit dislocations in our strained sample at low temperatures ($T \leqslant$ 80–100 K), and free-excitonic luminescence [7, 5] at higher temperatures.

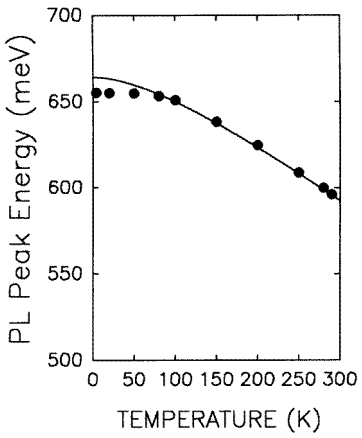

Figure 3. The temperature dependence of the PL peak energy for the $Ga_{0.75}In_{0.25}As_{0.04}Sb_{0.96}/Al_{0.22}Ga_{0.78}As_{0.02}Sb_{0.98}$ MQW structure. The solid curve was obtained by shifting the bulk $Ga_{0.75}In_{0.25}As_{0.04}Sb_{0.96}$ band gap to higher energies via the confinement energies, to coincide with the PL peak energy at room temperature.

In order to further analyse the origin of the PL emission at different temperatures from the quaternary structure, the luminescence characteristics were studied as functions of temperature and incident laser excitation density (I_0) over a range of three orders of magnitude. The integrated intensity of the luminescence peaks (I_{PL}) was found to obey $I_{PL} \propto I_0^{\alpha}$ with $\alpha = 1.05 \pm 0.05$ over the whole measured temperature range (4.0–290.0 K), which reveals radiative recombination to be the prevailing recombination process in the GaInAsSb/AlGaAsSb system, and excitonic PL to dominate the radiative process up to room temperature. This result is also in agreement with the absorption spectra which exhibit strong excitonic absorption even at room temperature. Figure 3 illustrates the temperature dependence of the luminescence peak energy. The solid curve was obtained by fitting the luminescence peak energy at 290.0 K to the bulk $Ga_{0.75}In_{0.25}As_{0.04}Sb_{0.96}$ band gap. When the temperature was decreased, the peak energy first increased, following the temperature dependence of the bulk $Ga_{0.75}In_{0.25}As_{0.04}Sb_{0.96}$ band gap down to around 100 K, and then deviated to the lower-energy side at low temperatures (by 9.0 meV at 4 K), keeping almost constant in the 4–80 K range. The above temperature-dependent behaviour of the luminescence peak energy suggests two possible explanations. First, that the recombination gradually evolves from excitonic to band-to-band type over a temperature range of 80–100 K, and the deviation amounts to the free-exciton binding energy. This seems unlikely, however, as the luminescence intensity depends linearly on the excitation power intensity up to room temperature. An alternative explanation is that the luminescence peaks can be ascribed to free-exciton recombination from 80 to 100 K up to room temperature, while exciton trapping to disorder and interface defects dominates at low temperatures, and the deviation amounts to the exciton–defect binding energy, in agreement with the case of the temperature-dependent Stokes shift behaviour described above. The exciton–defect binding energy of $\sim$9.0 meV is also consistent with the value reported in the literature [23]. Unlike other authors [5, 7], we cannot distinguish the excitons and localized excitons purely from their binding energies in our sample; however, the dependence on excitation power and temperature of the PL characteristics and the symmetrical luminescence line shape at temperatures below 250 K strongly demonstrates the reliability of the latter explanation.

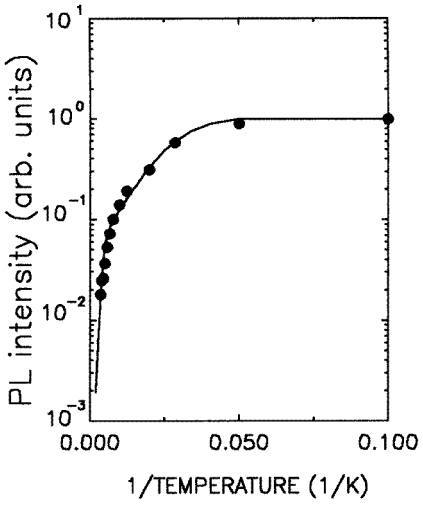

Figure 4. An Arrhenius plot of $\log(I_{PL})$ as a function of inverse temperature for the quaternary $Ga_{0.75}In_{0.25}As_{0.04}Sb_{0.96}/Al_{0.22}Ga_{0.78}As_{0.02}Sb_{0.98}$ strained MQW structure. The laser power density was 100 mW cm^{-2} for the PL measurements. The solid line was fitted to the experimental data by using equation (13).

4.4. The luminescence quenching mechanism

With increase in temperature, the integrated luminescence intensity decreases, indicating the presence of nonradiative recombination mechanisms. The log of the measured PL integrated intensity is plotted as a function of inverse temperature in figure 4. The PL intensity reduces by only ∼50 in magnitude when the temperature is increased from 10 to 290 K, which confirms the radiative recombination to be prevailing in the GaInAsSb/AlGaAsSb system up to room temperature, and has been normalized to the maximum intensity of 10 K. The sample clearly shows the temperature-dependent behaviour characterized by two temperature regimes, corresponding to two thermally activated nonradiative recombination mechanisms. The solid line is the best fit to the experimental data, with a model involving two nonradiative recombination processes described by [23, 26]

$$I_{nor} = \left[1 + C_1 \exp\left(-\frac{E_1}{K_B T}\right) + C_2 \exp\left(-\frac{E_2}{K_B T}\right)\right]^{-1} \tag{13}$$

where I_{nor} is the normalized PL intensity, C_1 and C_2 are constants, E_1 and E_2 are the thermal activation energies, K_B is the Boltzmann constant, and T is the sample temperature. The best fit yields values of C_1, C_2 of 25.2, 12 000.0, and activation energies E_1, E_2 of 9.5 ± 0.5 meV, 135.0 ± 0.5 meV, respectively. The value of E_1 is in excellent agreement with the exciton–defect binding energy of ∼9.0 meV. The activation energy E_2 is consistent with the calculated value of 133.5 meV, the sum of the differences between the first and second electron subbands and between that of heavy-hole subbands. Therefore, we can conclude that the dominant decrease in luminescence in this quaternary system is mainly due to the trapped excitons thermalizing from the localized regions below 100 K, and the thermal excitation of carriers from the first electron and heavy-hole subbands to their second subbands at higher temperatures. Further evidence of the thermal excitation of carriers is that the PL spectra gradually change from a symmetrical line shape to an asymmetrical one at temperatures above 250 K (see the room temperature PL spectrum in figure 2),

when the luminescence signal on the high-energy side increases. However, we cannot observe luminescence peaks originating from the higher subbands, e.g., 1e–2hh and 2e–1hh, in contrast to the case for modulation-doped structures where the contribution from the thermal excitation carriers can also be observed [27] due to the spatial separation of the electrons and holes in the asymmetric system, which weakens the parity selection rule $\Delta n = 0$.

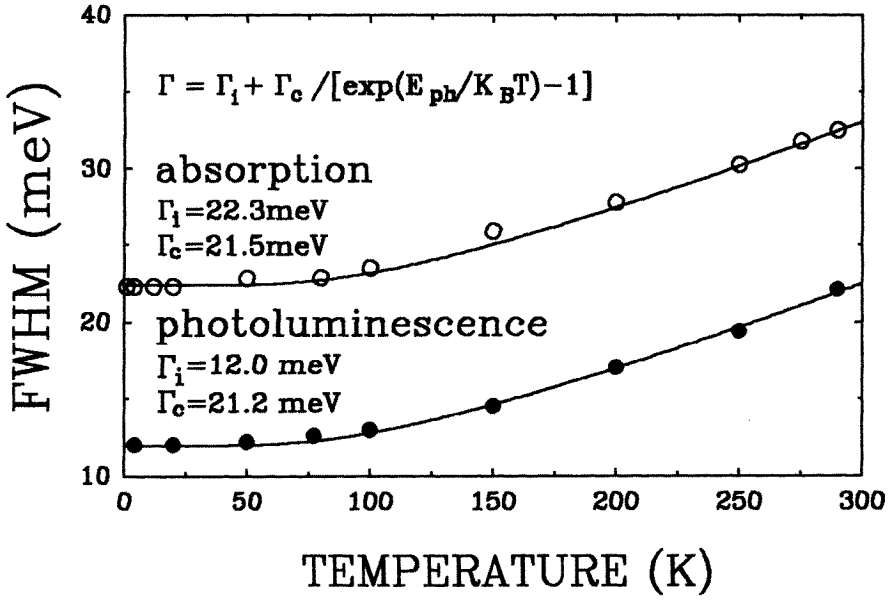

Figure 5. The photoluminescence and absorption linewidth (FWHM) for the quaternary $Ga_{0.75}In_{0.25}As_{0.04}Sb_{0.96}/Al_{0.22}Ga_{0.78}As_{0.02}Sb_{0.98}$ strained MQW as functions of temperature. The solid lines were calculated using the exciton–optical-phonon coupling model.

4.5. Linewidth analysis

The temperature dependence of the luminescence and absorption linewidth (FWHM) in the quaternary MQW is shown in figure 5. The measured luminescence line shape is a convolution of an inhomogeneous part with FWHM Γ_i and a temperature-dependent homogeneous part (FWHM Γ_h). The inhomogeneous linewidth is mainly due to the interface roughness, random alloy disorder, and well width fluctuations. Since no impurity transition is involved in the low-energy side of the luminescence peaks due to the symmetrical PL line shape at low temperatures, the inhomogeneous broadening due to the scattering by impurities has not been taken into account. At low temperatures, the scattering by longitudinal acoustic (LA) phonons dominates the temperature-dependent term. However, its contribution to the line shape can be neglected in QW structures [28]. As the temperature increases, scattering by longitudinal optical (LO) phonons becomes dominant due to the increasing phonon population, which gives rise to the homogeneous part of the linewidth broadening. In contrast to the band-to-band transition case where the FWHM increases linearly with temperature [23], the measured FWHM data here can be well fitted with an exciton–optical-phonon coupling model in which free excitons scatter off LO phonons [29] by the following

expressions:

$$\Gamma = \Gamma_i + \Gamma_h$$
$$\Gamma_h = \Gamma_c \left[\exp\left(\frac{E_{ph}}{K_B T} \right) - 1 \right]^{-1} \tag{14}$$

where Γ_c is a measure of the exciton–phonon coupling and the value of $E_{ph} = 28.55$ meV is the LO phonon energy in $Ga_{0.75}In_{0.25}As_{0.04}Sb_{0.96}$ obtained by linear interpolation (see equation (3)).

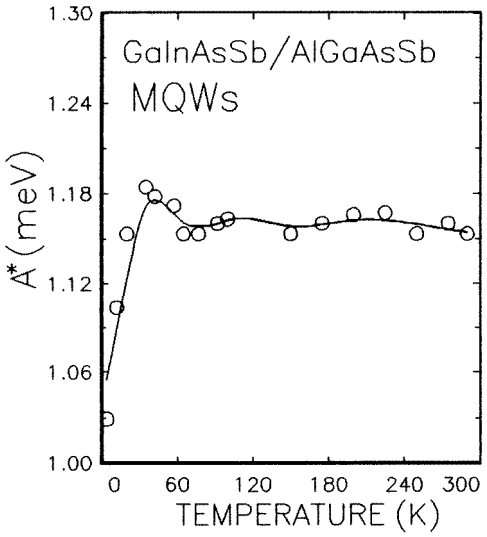

Figure 6. The quantity $A^* = \int A(E)\ \mathrm{d}E$ (E is the photon energy) for the 1e–1hh absorption peak as a function of temperature for the GaInAsSb/AlGaAsSb MQW structure. The solid line is a guide to the eye.

The excellent fit gives $\Gamma_i = 12.0$ meV and $\Gamma_c = 21.2$ meV for the luminescence linewidth, and $\Gamma_i = 22.3$ meV and $\Gamma_c = 21.5$ meV for the absorption linewidth. At low temperatures, splitting of the 1e–1hh peak was observed in the absorption spectra (see, e.g., the 4.0 K absorption spectrum in figure 2), with the energy spacing of 4.5 meV due to the well width fluctuations of about 1.8 monolayers based on theoretical calculation. Furthermore, the scattering from the random alloy disorder in the quaternary system at low temperatures would be large. The above two aspects would lead to the value of Γ_i (12.0 meV). The well width fluctuations at interfaces and random alloy disorder scattering would also result in the localization of excitons at low temperatures. The contribution from the interface roughness would be small, due to the strong luminescence intensity of the sample. The value of Γ_i (12.0 meV) is much smaller than that obtained by fitting from the absorption spectra (22.3 meV) due to the different transition mechanisms between them, i.e., the recombination luminescence decreases exponentially when the photon energy is larger than the PL peak energy, while all of the energy states can be involved in the absorption spectra [30]. However, the value Γ_c of 21.2 meV is in excellent agreement with that estimated from the absorption measurements (21.5 meV), indicating that the exciton–phonon coupling in the GaInAsSb/AlGaAsSb system is relatively strong, which should be taken into account in exciton-based devices. Furthermore, the LO phonon contribution to

the line shape Γ of 9.9 meV at room temperature is close to the free-exciton binding energy ($\sim$10 meV), which confirms that excitonic states are not ionized and that the PL peak is related to free-exciton recombination up to room temperature. In addition, exciton lifetimes are estimated from the homogeneous linewidth using the uncertainty principle; it implies a mean exciton ionization time of the order of 60 fs at room temperature.

4.6. The excitonic polariton

Excitonic polaritons in optical absorption in bulk GaAs and GaAs/AlGaAs MQW structures have been reported by Kosobukin *et al* [31]. We have also reported the observation of excitonic polariton absorption in InGaAs/GaAs strained QWs [32]. Figure 6 shows the quantity $A^* = \int A(E)\ \mathrm{d}E$ for the 1e–1hh absorption peak as a function of temperature for the quaternary GaInAsSb/AlGaAsSb MQW sample, where we have employed $A(E)$ (absorption in the exciton absorption band) instead of the absorption coefficient because we do not know the exact thickness of the sample. The formation of polaritons makes the thin semiconductor structures more transparent at low temperatures up to the critical temperature T^*, at which the exciton damping parameter (Ω) reaches its critical value (Ω_c). Since the quantity A^* is proportional to Ω for $\Omega < \Omega_c$ and does not depend on Ω for $\Omega > \Omega_c$ [31], on further increasing the temperature, the integral over the excitonic absorption band will keep at a constant, A^*_{max}. In figure 6, we have actually observed A^* to increase rapidly up to $\sim$40 K and then remain nearly constant up to room temperature, which is typical of the excitonic-polariton–mechanical-exciton transition in absorption [31, 32]. This observed effect is likely to be due to the slight deviation from normal incidence.

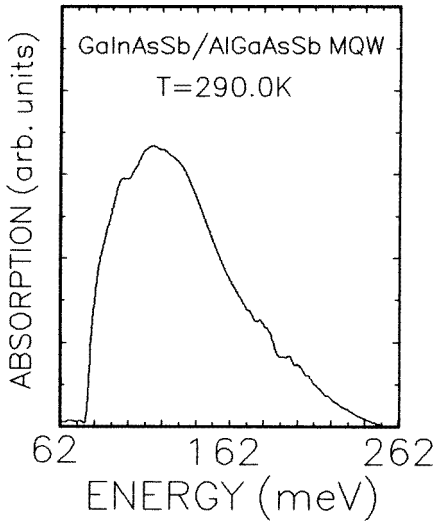

Figure 7. The infrared absorption spectrum for the same GaInAsSb/AlGaAsSb MQW structure at 290 K, showing an intersubband absorption at around 10.7 μm.

4.7. Intersubband transition

Figure 7 shows the normal-incidence intersubband absorption spectrum for the same MQW sample at room temperature. The absorption peak centred at 115.9 meV (10.7 μm), corresponding to the transition between the first conduction subband and second conduction subband (1e–2e) within the conduction band of $Ga_{0.75}In_{0.25}As_{0.04}Sb_{0.96}$ wells, is in good

agreement with the theoretical intersubband calculation for the 1e–2e transition energy of 113.5 meV (10.9 μm). The charge in the conduction bands is thermally generated at high temperatures. Further confirmation of the assignment was obtained from the experimental facts that the absorption peak location did not shift with the decrease of temperature. On the basis of our calculation, the second electron subband level nearly reaches the top of the wells, together with the wider subband levels, due to the stronger alloy random scattering; these two aspects result in a wider intersubband absorption linewidth (6.3 μm), which reveals the suitability of quaternary QWs in QWIPs.

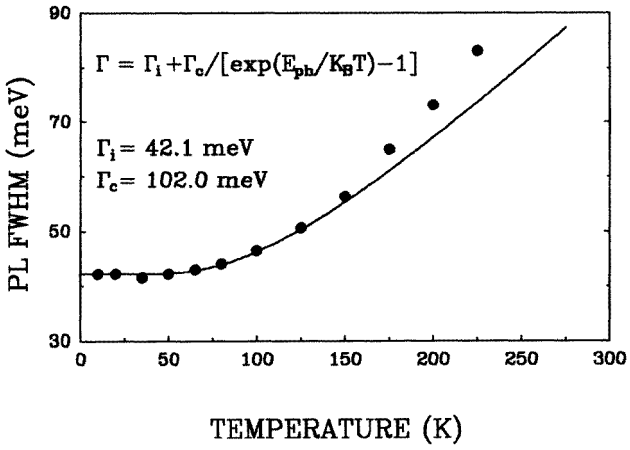

Figure 8. The photoluminescence linewidth (FWHM) for a quaternary $Ga_{0.67}In_{0.33}As_{0.01}Sb_{0.99}$/$Al_{0.25}Ga_{0.75}As_{0.02}Sb_{0.98}$ strained SQW structure as a function of temperature under the laser excitation density of 500 mW cm^{-2}. The solid line was calculated using the exciton–LO-phonon coupling model.

4.8. Thermal ionization of excitons in the SQW structure

Detailed PL and absorption studies of the SQW structure show that the origin of the PL emission and the luminescence quenching mechanism are similar to those in the MQW case. However, in comparison with the MQW case, linewidth analysis reveals some different results. Figure 8 shows the temperature-dependent luminescence linewidth in the SQW structure, together with the exciton–optical-phonon coupling fit (see equation (14)). The LO phonon energy $E_{ph} = 27.97$ meV for $Ga_{0.67}In_{0.33}As_{0.01}Sb_{0.99}$. We can see that the measured FWHM data below 150 K can be well fitted by the coupling model, giving $\Gamma_c = 102.0$ meV, which is much larger than that in the quaternary MQW case (21.2 meV), demonstrating that the exciton–phonon coupling in the GaInAsSb/AlGaAsSb SQW system is stronger than in the MQW structure. A similar result has been observed for InGaAs/GaAs QWs and attributed as being due to the alteration of the symmetric behaviour of the phonon vibration modes on the basis of the existence of periodicity in the growth direction in MQW structures [32]. The LO phonon contribution to the line shape Γ of 25.1 meV at 200 K is much larger than the free-exciton binding energy ($\sim$10 meV), and the exciton lifetimes are estimated to be about 26 fs at 200 K. The higher kinetic energy and shorter ionization time reveal the reality of thermal ionization of excitonic states at higher temperatures.

Further evidence of the thermal ionization of excitons is demonstrated in figure 9 which

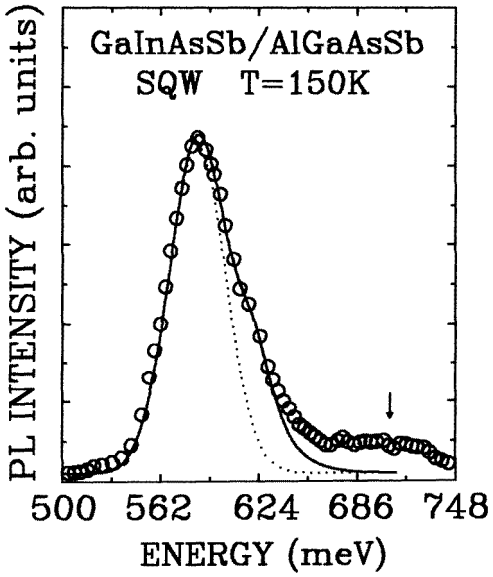

Figure 9. The photoluminescence spectrum line shape (open circles) and the best fit obtained using equations (3) and (4) with the appropriate parameters (solid curve) for a quaternary $Ga_{0.67}In_{0.33}As_{0.01}Sb_{0.99}/Al_{0.25}Ga_{0.75}As_{0.02}Sb_{0.98}$ strained SQW structure at 150 K with the laser excitation density of 500 mW cm^{-2}. The contribution of the exciton recombination is shown by a dotted curve. The calculated energy position of the 2e–1hh transition is marked by the arrow.

gives the detailed PL line-shape fit. The open circles show the experimental results at 150 K under lower excitation density (500 mW cm^{-2}). The dotted curve shows the calculated exciton recombination (I_{ex}) weighted by the following Gaussian function profiles:

$$I_{ex}(\hbar\omega) = A_{hh}\exp\left[-\frac{[\hbar\omega - E_{hh}(T)]^2}{2\sigma_{hh}^2(T)}\right]\exp\left(-\frac{\hbar\omega}{K_BT}\right) \tag{15}$$

where A_{hh}, E_{hh}, and σ_{hh} are the amplitude, energy, and broadening parameters of the 1e–1hh exciton recombination, respectively. We can see that the high-energy tail of the PL spectrum extends for several tens of meV from the Gaussian fitting results, in contrast to the excellent fit on the low-energy side of the PL spectrum. This deviation is due to the thermal ionization of excitons and recombination from free carriers [25]. The possibility of exciton recombination without exciton wave-vector conservation can be excluded for our 10 nm well layer [25]. Therefore, we have also taken into account the contribution of free-carrier recombination [25] (I_{bb}) in the fitting process:

$$I_{bb}(\hbar\omega) = A_{bb}\frac{1}{1+\exp[-(\hbar\omega - E_{bb}(T)/\sigma_{bb}(T))]} \times \frac{2}{1+\exp[-2\pi\sqrt{R/(\hbar\omega - E_{bb}(T))}]}\exp\left(-\frac{\hbar\omega}{K_BT}\right) \tag{16}$$

where A_{bb}, E_{bb}, and σ_{bb} are the amplitude, band-to-band transition energy, and broadening parameters of the free-carrier recombination, respectively. R is the exciton binding energy. The best fit is shown in figure 9 by a solid curve, which clearly shows the presence of band-to-band recombination. Furthermore, it is the partial ionization of excitons at higher

temperatures (above 125 K) that makes the PL linewidth deviate from the exciton–phonon coupling model (see figure 8). In addition, we think that the luminescence signal above 0.650 eV originates from the higher electron subbands (2e–1hh), on the basis of its energy position (the calculated result is marked by the arrow in figure 9). Since the PL spectrum in figure 9 was recorded under lower excitation density, the appearance of the 2e–1hh transition here is due to the thermal excitation of carriers at higher temperatures rather than the band-filling effect, reinforcing the conclusion of luminescence quenching reached above.

5. Conclusion

With the aid of the temperature-dependent PL and absorption measurements, we have determined that radiative recombination governs the recombination mechanism and that excitonic PL dominates the radiative process for GaInAsSb/AlGaAsSb strained QW structure grown by MBE, in addition to demonstrating their good quality. The PL peaks can be ascribed to free-exciton recombination above 100 K while localized excitons dominate at low temperatures. The dominant luminescence quenching mechanism in this quaternary system is mainly the trapped excitons thermalizing from the localized regions below 100 K, and the thermal carrier activation from the first electron and heavy-hole subbands to the second electron and heavy-hole subbands at higher temperatures. Theoretical calculations including both the strain and confinement effects agree well with the measurement results, leading to the conclusion that the $Ga_{0.75}In_{0.25}As_{0.04}Sb_{0.96}/Al_{0.22}Ga_{0.78}As_{0.02}Sb_{0.98}$ MQW is normal type I for light holes, and the conduction band offset ratio $Q_c = 0.66 \pm 0.01$. The transition from type I to type II for light holes is predicted theoretically. The exciton line broadening with temperature is explained on the basis of the exciton–LO-phonon coupling model, in which the strength of the exciton–phonon coupling is determined. Evidence for excitonic polariton absorption in GaInAsSb/AlGaAsSb MQW structures is obtained from the experimental fact that the integral over the excitonic absorption edge, representing the exciton damping parameter, increases from a low value at low temperature to a constant value at a critical temperature T^* of $\sim$40 K. Intersubband infrared absorption within the conduction band (1e–2e) has been observed. We have demonstrated the thermal ionization of excitons in SQW structures at higher temperatures (above 125 K) due to the stronger exciton–LO-phonon coupling, with the aid of PL line-shape analysis which clearly shows the presence of band-to-band recombination. We believe that the results obtained in this paper for the GaInAsSb/AlGaAsSb strained QW structure will be useful in the development and design of new devices based on these quaternary materials and their microstructures.

References

[1] See, e.g.,
Dingle R, Wiegmann W and Henry C 1974 *Phys. Rev. Lett.* **14** 827
[2] Lambkin J D, Dunstan D J, Homewood K P, Howard L K and Emeny M T 1990 *Appl. Phys. Lett.* **57** 1986
[3] Michler P, Hangleiter A, Moser M, Geiger M and Scholz F 1992 *Phys. Rev.* B **46** 7280
[4] Marcinkevičius S, Olin U and Treideris G 1993 *J. Appl. Phys.* **74** 3587
[5] Dotor M L, Recio M, Golmayo D and Briones F 1992 *J. Appl. Phys.* **72** 5861
[6] Ding Y J, Guo C L, Li S, Khurgin J B, Law K K and Merz J L 1992 *Appl. Phys. Lett.* **60** 154, 2051
[7] Fujiwara K, Tsukada N and Nakayama T 1988 *Appl. Phys. Lett.* **53** 675
[8] Lines M E 1984 *Science* **226** 663
[9] France R W, Carter S F, Williams J R, Beales K J and Parker J M 1984 *Electron. Lett.* **20** 607
[10] Bochkarev A E, Dolginov L M, Drakin A E, Eliseev P G and Sverdlov B N 1988 *Sov. J. Quantum Electron.* **18** 1362
[11] Baranov A N, Imenkov A N, Mikhailova M P, Rogachev A A and Yakovlev Y P 1989 *Proc. SPIE* **1048** 188

[12] Chiu T H, Tsang W T, Ditzenberger J A and van der Ziel J P 1986 *Appl. Phys. Lett.* **49** 1051
[13] Eglash S J and Choi H K 1990 *Appl. Phys. Lett.* **57** 1292
[14] Adachi S 1987 *J. Appl. Phys.* **61** 4869
[15] Adachi S 1985 *J. Appl. Phys.* **58** R1
[16] Miller D A B, Chemla D S, Damen T C, Wood T H, Burrus C A, Gossard A C and Wiegmann W 1985 *IEEE J. Quantum Electron.* **21** 1462
[17] West L C and Eglash S J 1985 *Appl. Phys. Lett.* **46** 1156
[18] Levine B F 1993 *J. Appl. Phys.* **74** R1
[19] See, e.g.,
Long D 1968 *Energy Bands in Semiconductors* (New York: Interscience)
Casey H C Jr and Panish M B 1978 *Heterostructure Lasers* (New York: Academic) Part B
[20] Pollak F H and Cardona M 1968 *Phys. Rev.* B **172** 816
[21] Pollak F H 1990 *Semiconductors and Semimetals* vol 32, ed T P Pearsall (San Diego, CA: Academic) p 17
[22] Cheng M J, Stringfellow G B, Kisker D W, Srivastava A K and Zyskind J L 1986 *Appl. Phys. Lett.* **48** 419
[23] Iyer S, Hegde S, Abul-Fadl A, Bajaj K K and Mitchel W 1993 *Phys. Rev.* B **47** 1329
[24] Delalande C, Meynadier M H and Voos M 1985 *Phys. Rev.* B **31** 2497
[25] Colocci M, Gurioli M and Vinattieri A 1990 *J. Appl. Phys.* **68** 2809
[26] Lambkin J D, Considine L, Walsh S, O'Connor G M, McDonagh C J and Glynn T J 1994 *Appl. Phys. Lett.* **65** 73
[27] Yu P W, Jogai B, Rogers T J, Martin P A and Ballingall J M 1994 *J. Appl. Phys.* **76** 7535
[28] Lee J, Kotcles E S and Vassel M O 1986 *Phys. Rev.* B **33** 5512
[29] Bebbs H B and Williams E H 1972 *Semiconductor and Semimetals* vol 8, ed R K Willardson and A C Beer (New York: Academic) p 256
[30] Shen S C 1992 *Optical Properties in Semiconductors* (Beijing: Science) ch 5 p 311 (in Chinese)
[31] Kosobukin V A, Seisyan R P and Vaganov S A 1993 *Semicond. Sci. Technol.* **8** 1235
[32] Shen W Z, Shen S C, Tang W G, Wang S M and Andersson T G 1995 *J. Phys.: Condens. Matter* **7** L79; *J. Appl. Phys.* **78** 1178
[33] Ji G, Huang D, Reddy U K, Henderson T S, Houdre R and Morkoc H 1987 *J. Appl. Phys.* **62** 3366
[34] Adachi S 1982 *J. Appl. Phys.* **53** 8775
[35] *Numerical Data and Functional Relationships in Science and Technology (Landolt–Börnstein New Series)* 1982 vols 17a and 17b, ed O Madelung, M Schulz and H Weiss (New York: Springer)
[36] People R and Jackson S A 1990 *Semiconductors and Semimetals* vol 32, ed T P Pearsall (San Diego, CA: Academic) p 154
[37] Pankove J I 1971 *Optical Processes in Semiconductors* (Englewood Cliffs, NJ: Prentice-Hall) p 412